Journal of Optoelectronics and Advanced Materials Vol. 6, No. 1, March 2004, p. 225 - 235

A NEW X-RAY LINE PROFILE APPROXIMATION USED FOR THE EVALUATION OF THE GLOBAL NANOSTRUCTURE OF NICKEL CLUSTERS♣

N. Aldea*, C. V. Tiusan, B. Barz

National Institute for Research and Development of Isotopic and Molecular Technology
P.O. Box 700, 3400 Cluj-Napoca, Romania

The analysis of the diffraction line broadening in X-ray powder pattern is analytically calculated using the Generalized Fermi Function facilities. X-ray line broadening investigations of supported catalysts have been limited to finding the average crystallite size from the integral width or the full width at half maximum of the diffraction line. In the case of supported metal catalysts, it is generally difficult to perform satisfactory intensity measurements of the higher order *(hkl)* reflections. Consequently, the classical method of Warren and Averbach cannot be applied. In our cases, only one line is present in the experimental spectra, so we used an approximation method of Charlson that can be applied for small crystallite size. We present a new fitting method based on the Generalized Fermi Function for the approximation and Fourier transform of the experimental X-Ray line profiles.

(Received September 20, 2003; accepted February 18, 2004)

Keywords: Supported metal catalysts, Crystallite size, X-Ray diffraction, Fourier transform

1. Introduction

The X-ray powder pattern diffraction profile broadening analysis is a valuable technique for the crystalline materials structure and properties investigation. The powder reflection broadening of the metal support catalyst is normally caused by small size crystallites and by distortions within crystallites due to dislocation configurations [1,2]. The structural information obtainable by single X-ray profile Fourier transform consist in: effective particle size, microstrains, particle distribution function and stacking fault probability. These information were obtained by numerical deconvolution of the instrumental and experimental X-Ray line profiles (XRLP) approximated by Generalized Fermi Function (GFF) [3-5].

The XRLP Fourier analysis validity depends strongly on the magnitude and nature of the errors propagated in analysis [6]. Herein, we emphasize only sampling factors such as evaluation of the background corrections, angular range of the observation and the number of equally spaced points at which the diffraction line intensity is measured. This type of errors was recently treated [7]. Our analytical approach, adopted here, eliminates all these errors.

2 Why do we use GFF for the XRLP analysis?

It is known that, from a mathematical point of view, XRLP are described by an asymmetric function [1]. In the papers published by Balzar, Cheary, Toraya and Young [8-11] a large variety of functions for analysis of the XRLP such as Voigt (V), pseudo-Voigt (pV) or Pearson VII (P7) are proposed. They have the forms

---

♣ Presented at Romanian Conference of Advanced Materials, Constanta, Romania, September 15-18, 2003

* Corresponding author: naldea@L30.itim-cj.ro

$$V(s) = \frac{a_1 \int_{-\infty}^{\infty} \frac{\exp(-y^2)}{a_4^2 + \left(\frac{s-a_2}{a_3} - y\right)^2} dy}{\int_{-\infty}^{\infty} \frac{\exp(-y^2)}{a_4^2 + y^2} dy}, \tag{1}$$

$$pV(s) = b_2 \left\{ \frac{b_1}{1 + \left(\frac{s-b_3}{b_4}\right)^2} + (1-b_1) \exp\left[-\frac{1}{2} \left(\frac{s-b_3}{b_4}\right)^2 \right] \right\}, \tag{2}$$

$$P7(s) = \frac{c_1}{\left[1 + 4\left(\frac{s-c_2}{c_3}\right)\left(2^{1/c_4} - 1\right) \right]^{c_4}}, \tag{3}$$

where $s = 2\sin\theta/\lambda$ is the module of the wave vector. The values (a_1, b_2, c_1), (a_2, b_2, c_2), (a_3, b_3, c_3) describe the amplitude, the position and the shape of the peak, respectively. The parameter a_1 from $pV(s)$ gives a mixing ratio of Lorentzian contribution to the Gaussian. Denominator of $V(s)$ distribution can be expressed as

$$\int_{-\infty}^{\infty} \frac{\exp(-y^2)}{a_4^2 + y^2} dy = [1 - \Phi(a_4)] \frac{\pi}{a_4} \exp(a_4^2), \tag{4}$$

where Φ is the integral of probability defined by the relationship

$$\Phi(a_4) = \frac{2}{\sqrt{\pi}} \int_0^{a_4} \exp(-t^2) dt. \tag{5}$$

Although extensive research over the past few decades has made progress in the XRLP global approximations, their complete analytical properties were not reported in literature. Unfortunately, most of them have complicated forms and they are not easy to handle mathematically. Recently [12,15] a simple function with a minimal number of parameters named generalized Fermi function, suitable for minimization and having remarkable analytical properties was presented from a purely phenomenological point of view. It is given by the relationship,

$$h(s) = \frac{A}{e^{-a(s-c)} + e^{b(s-c)}} \tag{6}$$

where A, a, b, c are unknown parameters. The values A, c describe the amplitude and the position of the peak, a, b control its shape. If $b=0$, the h function reproduces the Fermi-Dirac electronic energy distribution.

2.1 The main properties of the *h* function

The GFF has remarkable mathematical properties, with direct use in determining the moments, the integral width, the Fourier transform of the XRLP or the true sample function, respectively. Here we give its properties without proofs.

(1) if we put $a = b$, the function h is a symmetric curve around the c value, therefore $h(-s+c) = h(s+c)$;

(2) let a,b,c be fixed; the coordinates of the h function maximum reported to c value, are $(\xi+c, \eta)$ where

$$\xi = \frac{\ln\frac{a}{b}}{a+b},\ \eta = A\frac{(a^a b^b)^{1/(a+b)}}{a+b}\ ;$$

(3) if we set $s = c$ we obtain

$$h(c) = \frac{A}{2};$$

(4) by setting $s' = s - c$, $\rho = (a + b)/2$ and $q = (a - b)/2$, we have

$$h(s') = \frac{A}{2}\left(\frac{\cosh qs' + \sinh qs'}{\cosh \rho s'}\right); \tag{7}$$

(5) the limit of $h(s')$ function for infinite arguments is finite, so that

$$\lim_{s'\to\pm\infty} h(s') = 0;$$

(6) the zero, the first and the second order moments (μ_0, μ_1, μ_2) of the h function are given by the relationships

$$\mu_0 = \frac{\pi A}{2\rho\cos\frac{\pi q}{2\rho}},\ \mu_1 = \frac{\pi}{2\rho}\tan\frac{\pi q}{2\rho}, \mu_2 = \left(\frac{\pi}{2\rho}\right)^2 \frac{1}{\cos^2\frac{\pi q}{2\rho}}; \tag{8}$$

(7) the integral width $\delta_h(a, b)$ of the h function has the following form

$$\delta_h(a,b) = \frac{\pi}{(a^a b^b)^{1/(a+b)}\cos\left(\frac{\pi}{2}\frac{a-b}{a+b}\right)}; \tag{9}$$

(8) the Fourier transform of the h function is given by the relationship

$$H(L) = \frac{A}{2}\int_{-\infty}^{\infty}\frac{\cosh qs' + \sinh qs'}{\cosh \rho s'} e^{-2\pi s' L} ds' = \frac{\pi A}{2\rho\left|\cos\left(\frac{\pi q}{2\rho} + i\frac{\pi^2 L}{\rho}\right)\right|^2}\cos\left(\frac{\pi q}{2\rho} - i\frac{\pi^2 L}{\rho}\right); \tag{10}$$

(9) if we consider the functions f and g defined by equation (7), their convolution product is the h function defined as

$$h(s) = \int_{-\infty}^{\infty} f(s-t)g(t)dt, \tag{11}$$

where h represents the experimental XRLP, f is the true XRLP of the sample and g is the instrumental function. If we consider the well known relations between the Fourier transforms of the functions h, f and g, we can compute the $|F(L)|$ function [1] which is used in Warren and Averbach analysis [16]. Therefore, the magnitude of $F(L)$ function has the following form

$$|F(L)| = \frac{A_h \rho_g}{A_g \rho_h}\sqrt{\frac{\cos^2\alpha + \sinh^2\beta L}{\cos^2\gamma + \sinh^2\delta L}}, \tag{12}$$

where the arguments of trigonometric and hyperbolic functions are expressed by

$$\alpha = \frac{\pi q_g}{2\rho_g},\ \beta = \frac{\pi^2}{\rho_g},\ \gamma = \frac{\pi q_h}{2\rho_h},\ \delta = \frac{\pi^2}{\rho_h}$$

The subscripts *g* and *h* refer to the instrumental and experimental XRLP. Taking into account the convolution theorem, the true sample function *f* is given by the relationship,

$$f(s) = \frac{A_h \rho_g}{A_g \rho_h} \int_{-\infty}^{\infty} \frac{\cos\left(\frac{\pi q_g}{2\rho_g} + i\frac{\pi^2 L}{\rho_g}\right)}{\cos\left(\frac{\pi q_h}{2\rho_h} + i\frac{\pi^2 L}{\rho_h}\right)} \exp(2\pi L s)\, dL \tag{13}$$

The last integral cannot be accurately resolved. In order to do this we have to consider some arguments. The Fourier transform of *f* is the *F* function, given by the relationship

$$F(L) = |F(L)| \exp(i\theta(L)) \quad \theta(L) = \arctan \frac{\Im|F(L)|}{\Re|F(L)|}$$

where θ means the angle function, $\Im|F(L)|$ and $\Re|F(L)|$ are the real and the imaginary part of the complex function *F*, respectively. The arguments α, β, γ and δ from equation (12), depend only on the asymmetry parameters *a* and *b* of the *g* and *f* functions. If the XRLP asymmetry is not very large (i.e. *a* and *b* parameters are closely enough as value) the $\cos^2\alpha \approx 1$, $\cos^2\gamma \approx 1$ approximations are reliable. The validity of these approximations will be illustrated in Table 2. Therefore we obtain $\Im|F(L)| << \Re|F(L)|$, θ (L) ≈ 0 and the magnitude of the Fourier transform for true XRLP sample can be expressed as

$$|F(L)| = \frac{A_h \rho_g}{A_g \rho_h} \frac{\cosh\frac{\pi^2 L}{\rho_g}}{\cosh\frac{\pi^2 L}{\rho_h}}; \tag{14}$$

(10) if we consider the previous approximation, the true XRLP sample is given by an inverse Fourier transform of the *F* function and consequently we have

$$f(s') = \frac{2A_h \rho_g}{\pi A_g} \frac{\cos\frac{\pi\rho_h}{2\rho_g}\cosh\rho_h s'}{\cosh 2\rho_h s' + \cos\frac{\pi\rho_h}{\rho_g}}; \tag{15}$$

(11) the integral width of the true XRLP sample can be expressed by the δ_f function

$$\delta_f(\rho_h, \rho_g) = \frac{\pi}{2\rho_h \cos\frac{\pi\rho_h}{2\rho_g}}\left(\cos\frac{\pi\rho_h}{\rho_g} + 1\right). \tag{16}$$

3. Theoretical background

The X-ray diffraction pattern of a crystal is described in the scattering intensity term, as a function of the scattering direction defined by the scattering angle *2 sin θ/λ*, where λ is the wavelength of the incident radiation. We shall assume case of the X-ray diffraction for a model mosaic structure

in which the atoms are arranged in blocks, each block itself being an ideal crystal, but with adjacent blocks not accurately fitted together. If *h(2θ)* is the measured diffracted peak profile, the $K_{\alpha 1}$ line is resolved by applying the Rachinger correction

$$h_{\overline{\alpha}}(2\theta) = h_{\alpha 1}(2\theta) + \frac{1}{2} h_{\alpha 1}(2\theta - \Delta 2\theta_{\alpha 1-\alpha 2}), \tag{17}$$

where $\Delta 2\theta_{\alpha 1-\alpha 2}$ is the angular doublet separation equal to

$$2\tan\theta \frac{\lambda(K_{\alpha 2}) - \lambda(K_{\alpha 1})}{\lambda}$$

and 2θ is the Bragg angle. The X-ray diffraction line profile is the convolution of the true data function $f_{\alpha 1}(s)$ by the instrumental function $g_{\alpha 1}(s)$ and is described by the Fredholm integral equation of the first kind given by equation (11). Warren et al. [16] have shown that for small *L* values, the Fourier transform of true sample function can be expressed as

$$\mathrm{F(L)} = \mathrm{A^s(L)A^{\varepsilon}(L)}, \tag{18}$$

where A^s function depends on the particle size and A^{ε} depends on the microstrain or distortion of the lattice. For cubic lattices, the functions A^s and A^{ε} can be expressed by the following relationships:

$$\mathrm{A^s}(L) = 1 - \frac{L}{D_{eff}(hkl)}$$

$$\mathrm{A^{\varepsilon}}(L) = 1 - \frac{2\pi^2 L^2 \left\langle \varepsilon^2(L) \right\rangle_{hkl} h_0}{a^2} \tag{19}$$

where *a* is the lattice parameter, *Deff* is the effective crystallite size along the normal to the *(hkl)* planes, $\left\langle \varepsilon^2(L) \right\rangle_{hkl}$ is the microstrain mean square averaged along the [*hkl*] direction and $h_0^2 = h^2 + k^2 + l^2$. Taking into account the experimental considerations presented in the preamble of the paper, for the case when only one line is presented in spectrum, we adopted the theory developed by Charlson et al. [2]. They shown that for small *L* values, the Fourier transform expression of the sample function is given by the relationship:

$$\mathrm{F}(L) = 1 - \frac{L}{D_{eff}} - C^2 \left\langle \varepsilon^2(L) \right\rangle_{hkl} L^2 + \frac{C^2 \left\langle \varepsilon^2(L) \right\rangle_{hkl} L^3}{D_{eff}}, \tag{20}$$

where $C^2 = 2\pi^2 h_0^2 / a^2$. By using a third order polynomial least squares fit *Deff* can be solved if the functional form $\left\langle \varepsilon^2(L) \right\rangle_{hkl}$ is known. Rothman et al. [17] assume the form of the strain function as

$$\left\langle \varepsilon^2(L) \right\rangle_{hkl} = \frac{K}{L}. \tag{21}$$

With this assumption, the new expression for *F* function has a second order polynomial form in *L*,

$$F(L) = a_0 + a_1 L + a_2 L^2 \tag{22}$$

where the a_0, a_1 and a_2 coefficients are defined as

$$a_0 \approx 1,\ a_1 = -\left(\frac{1}{D_{eff}} + C^2 K \right),\ a_2 = \frac{C^2 K}{D_{eff}}.$$

The best fit of equation (22) parameters is determined by the least square method. They are selected from condition $a_2 > 0$ requested by the inequality [1],

$$\frac{d^2F(L)}{dL^2} > 0\,. \tag{23}$$

The particle size distribution function *P(L)* described by Warren [1] and Aldea et al. [3], can be determined from the second order derivatives of the strain-corrected $A^s(L)$, with respect to *L*,

$$P(L) = D_{eff}\,\frac{d^2A^S(L)}{dL^2}\,, \tag{24}$$

where the function A^s can be obtained by the Warren et al. [16] method

$$A^S(L) = F(L)\exp\left(\frac{2\pi^2\left\langle\varepsilon^2(L)\right\rangle_{hkl}L^2}{d_{hkl}^2}\right). \tag{25}$$

The particle size distribution function can be used to calculate the average particle size using the following relations

$$\overline{D} = \int_{L_{\min}}^{L_{\max}} LP(L)dL\,, \tag{26}$$

$$D_{\perp} = \left(\int_{L_{\min}}^{L_{\max}} \frac{P(L)}{L}\,dL\right)^{-1}, \tag{27}$$

where $\overline{D}$ is the volumetric mean particle size and $D_{\perp}$ is the harmonical average of the particle thickness along the normal to the *(hkl)* reflecting planes.

The stacking fault probability $1.5\alpha+\beta$ (α = the sequence fault probability, β = the twin fault probability) can be calculated using the Wagner et al. [18] relationship

$$\frac{1}{D_{eff}} = \frac{1}{\overline{D}} + \frac{(1.5\alpha+\beta)V_{hkl}}{a}\,, \tag{28}$$

where *Vhkl* are the computed coefficients for the *fcc* lattice [1], if the presence of the distortions can be overlooked. Our data processing of the XRLP is consequently based on the previous theoretical consideration and on the GFF approximation and its properties.

4. Experimental

Our approach was tested on two samples of the supported on Al_2O_3 nickel catalysts (80 weight % *Ni*), treated at 350 ^oC and 850 ^oC in hydrogen atmosphere. Only order (111) of the intensities could be collected by a step-scanning constant acquisition time technique. Higher order reactions could not be measured due to the high dispersion degree of *Ni* crystallites. The observed diffraction profile of *Ni* foil sample considerate to be free of structural imperfection is used to represent the instrumental *g* function.

The X-ray (111) diffraction data of supported metal catalysts were collected using a horizontal powder diffractometer in Bragg-Brentano (BB) geometry with *Ni* filtered CuK_α radiation, λ = 1.54178 ° A, at room temperature. The typical experimental condition were: 90 sec. for each step, initial angle $2\theta = 42^0$, step 0.02^0 respectively and each profile was measured on 120 points. The diffraction profiles were measured with a proportional gas detector, single channel pulse-height discrimination and standard associated counting circuit.

5. Results and discussion

A new an efficient method for a global approximation of XRLP based on GFF has been proposed. Based on this simple approximation we could obtained the crystallites size, microstrain distribution functions and stacking fault probability of supported metal catalysts by using single X-Ray profile Fourier transform technique.

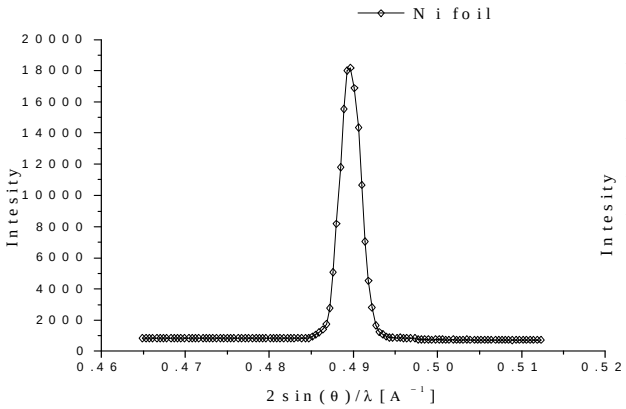

Fig. 1. The experimental relative intensity of the (111) $K_{\overline{\alpha}}$ for Ni foil.

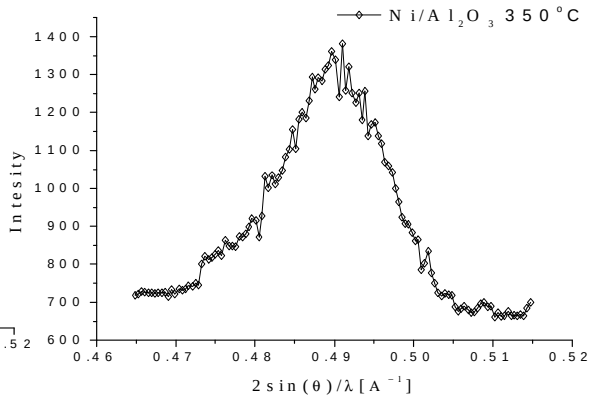

Fig. 2. The experimental relative intensity of the (111) $K_{\overline{\alpha}}$ f for Ni/Al_2O_3 350 °C.

Fig. 1 shows the instrumental line profile, obtained from the experimental *(111)* line of *Ni* foil, very well crystallized. The Figs. 2-3 show the experimental *(111)* lines for the samples presented in the previous section.

The experimental *(111)* XRLP were treated by the background and doublet corrections using our code XRLINE1, described by Aldea et al. [19]. Unfortunately, the best parameters of the XRLP can not be computed by the classical least square method because the GFF cannot be linearized. Therefore, the best parameters A, a, b, c for each XRLP were determined using the sequential simplex optimization procedure, based on the Nelder and Mead method [20].

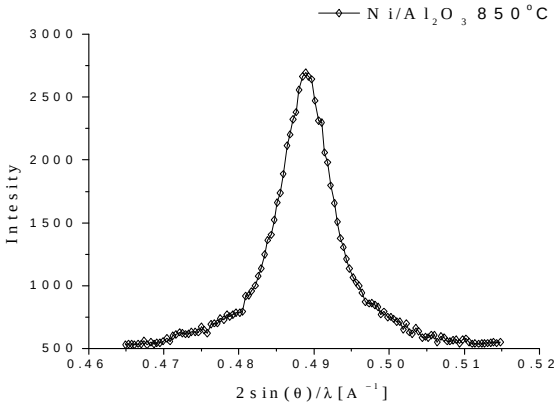

Fig. 3. The experimental relative intensity of the (111) $K_{\overline{\alpha}}$ for Ni/Al_2O_3 850 °C.

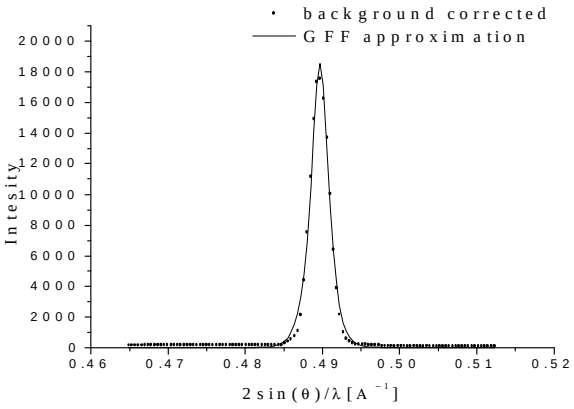

Fig. 4. The experimental relative (111) intensity, background and $K_{\overline{\alpha}}$ doublet corrected for Ni foil ,(…); fitted by GFF (solid line).

However, the question remains how does the XRLP and computational errors get distributed to each fitted parameter in analysis of the profiles. Our error analysis uses the equation for GFF approximation:

$$h(s) \pm \delta h = \frac{A \pm \delta A}{e^{-(a\pm\delta a)(s-(c\pm\delta c))} + e^{(b\pm\delta b)(s-(c\pm\delta c))}}, \tag{29}$$

where s is module of the wave vector, δA is uncertainty of the intensity, δa, δb are uncertainties of the shape parameters, and δc is uncertainty of the peak position. By knowing the fitted parameters A, a, b and c from the initial (unperturbed) simplex fit, one can keep these values constant in equation (29)

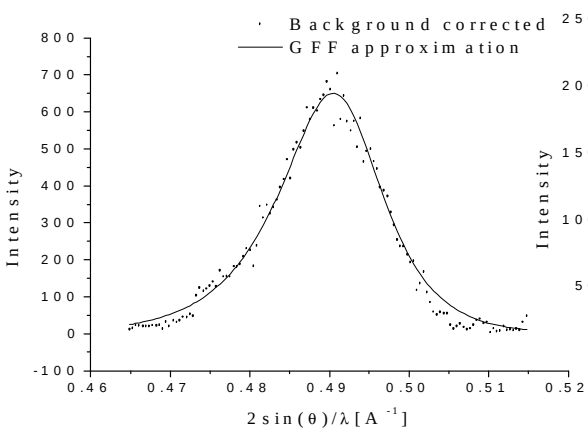

Fig. 5. The experimental relative (111) intensity, background and $K_{\overline{\alpha}}$ doublet corrected for Ni/Al_2O_3 350_oC ,(...); fitted by GFF (solid line).

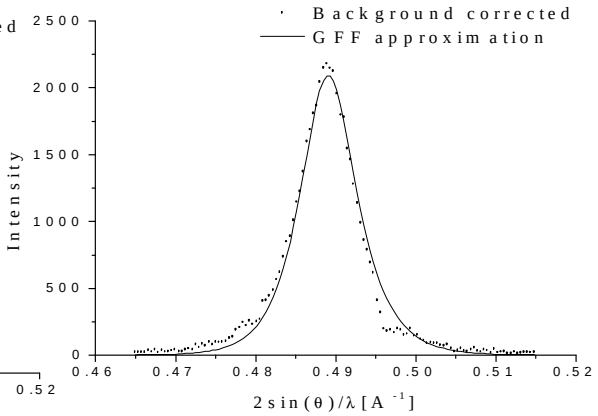

Fig. 6. The experimental relative (111) intensity, background and $K_{\overline{\alpha}}$ doublet corrected for Ni/Al_2O_3 850_oC ,(...); fitted by GFF (solid line).

and solve for δA, δa, δb and δc using the simplex procedure. The values δA, δa, δb and δc show how the XRLP errors distribute among the fitted parameters for GFF approximation. The discrepancy between the XRLP and GFF approximation is given by the residual index defined as,

$$R_{index} = \left(\frac{\sum_{i=1}^{np} (XRLP_i - GFF_i)}{\sum_{i=1}^{np} XRLP_i^2} \right)^{\frac{1}{2}}, \tag{30}$$

where *np* is number of the experimental points.

In order to compare validity of the GFF approximation with the classical distributions V, pV and P7 we followed the same procedures given by similar relations as (29) and (30). The best fit parameter values of each distribution, their uncertainties and residual indexes are reported in Table 1. By a compared analysis of the residual indexes we can observe that the GFF approximation has a low precision in approaching of the instrumental function but it has the best precision in fitting of all experimental XRLP. The Voigt distribution has the best precision in approximation of the narrowest broadening of the profiles such as instrumental function but it has a low precision for large integral widths. The pseudo-Voigt distribution has a acceptable residual index value for narrow profiles but it is not acceptable for profiles having medium and large integral widths. It has the worst precision for profiles having effective crystallite size greater than a hundred of angstroms. The residual index for Pearson VII distribution is valid for small and medium values of integral width but it is worse for profiles having a large broadening such as a crystalinity about some tens of angstroms.

Based on the best fit parameters and using properties 7 and 11 of the GFF approach, we determined the instrumental and true XRLP integral widths $\delta_g(\rho_h, \rho_g)$, $\delta_f(\rho_h, \rho_g)$. In order to further

justify our approximation $\cos^2\alpha \approx 1$, $\cos^2\gamma \approx 1$ adopted in property 9, we give the values for $\cos^2\alpha$, $\cos^2\gamma$ and the relative errors of the approximation in Table 2.

Table 1. The best parameters, uncertainties and residual indexes for all distributions.

GFF	A±δA	a±δa	b±δb	c±δc
g(s)	37117 ± 568.6	1029.24 ± 26.28	975.5 ± 45.05	$0.489 \pm 0.546 \times 10^{-4}$
$h(s)_{350^oC}$	1282.05 ± 14.65	146.766 ± 4.53	218.133 ± 8.328	$0.491 \pm 0.265 \times 10^{-3}$
$h(s)_{850^oC}$	4233.5 ± 28.435	284.946 ± 5.297	382.936 ± 9.460	$0.489 \pm 0.925 \times 10^{-4}$
V	$a_1 \pm \delta a_1$	$a_2 \pm \delta a_2$	$a_3 \pm \delta a_3$	$a_4 \pm \delta a_4$
g(s)	17897.5 ± 108.25	$0.49 \pm 0.75 \times 10^{-5}$	$0.0016 \pm 0.32 \times 10^{-5}$	$0.13 \pm 0.14 \times 10^{-3}$
$h(s)_{350^oC}$	631.695 ± 9.1	$0.489 \pm 0.24 \times 10^{-4}$	$0.008 \pm 0.3 \times 10^{-5}$	$0.267 \pm 0.26 \times 10^{-3}$
$h(s)_{850^oC}$	2147.93 ± 15.7	$0.488 \pm 0.33 \times 10^{-4}$	$0.019 \pm 0.26 \times 10^{-5}$	$1.709 \pm 0.8 \times 10^{-3}$
pV	$b_1 \pm \delta b_1$	$b_2 \pm \delta b_2$	$b_3 \pm \delta b_3$	$b_4 \pm \delta b_4$
g(s)	0.138 ± 0.026	17984.9 ± 107.1	$0.489 \pm 0.781 \times 10^{-5}$	$0.00123 \pm 0.81 \times 10^{-5}$
$h(s)_{350^oC}$	0.303 ± 0.062	638.9 ± 8.12	$0.489 \pm 0.87 \times 10^{-4}$	$0.0069 \pm 0.986 \times 10^{-4}$
$h(s)_{850^oC}$	0.034 ± 0.003	2062.9 ± 19.7	$0.488 \pm 0.403 \times 10^{-4}$	$0.0035 \pm 0.44 \times 10^{-4}$
P7	$c_1 \pm \delta c_1$	$c_2 \pm \delta c_2$	$c_3 \pm \delta c_3$	$c_4 \pm \delta c_4$
g(s)	17823.4 ± 117.44	$0.489 \pm 0.865 \times 10^{-5}$	$0.003 \pm 0.270 \times 10^{-4}$	26.056 ± 20.9
$h(s)_{350^oC}$	636.53 ± 8.004	$0.489 \pm 0.878 \times 10^{-4}$	$0.015 \pm 0.292 \times 10^{-3}$	3.711 ± 0.796
$h(s)_{850^oC}$	2155.43 ± 17.24	$0.488 \pm 0.28 \times 10^{-4}$	$0.0078 \pm 0.976 \times 10^{-4}$	1.662 ± 0.087
R_{index}[%]				
	GFF	V	pV	P7
g(s)	5.33	4.36	4.52	5.02
$h(s)_{350^oC}$	8.85	9.74	9.65	9.69
$h(s)_{850^oC}$	5.59	8.24	11.32	5.98

Table 2. The integral widths for instrumental function and true samples.

Name of sample	$\delta_g(a,b)$ [Å^{-1}]	$\delta_f(\rho_h,\rho_g)$ [Å^{-1}]	$\cos^2\alpha$	$\cos^2\gamma$	Rel. err. %
g(s)	0.00313	-	0.99786	-	0.21
$h(s)_{350C}$	-	0.01707	-	0.94217	5.78
$h(s)_{850C}$	-	0.00863	-	0.99472	0.52

The typical results for the background, doublet corrections of the XRLP and profiles resulting from GFF approximation are shown in Figs. 4-6.

Also, the microstructural parameters D_{eff}, $\langle\varepsilon^2\rangle_{hkl}$, D_{aritm}, D_{harm} and $1.5\alpha+\beta$ were calculated using relations (22), (21), (26), (27) and (28) for each distributions. Numerical results obtained from classical distributions are in good relations with parameters determined from GFF approach. The robustness of GFF approximation in this step of analysis arises from possibility to use the analytical form of Fourier transform given by relation (12) instead of the numerical Fourier transform. In order to connect the *V, pV, P7* distributions to relation (22) we had to execute their numerical Fast Fourier Transforms (FFT) because they do not have analytical formula. It is well known that validity of numerical FFT depend on the filtering technique adopted. In this way validity of the structural parameters are closely related to the accuracy of the FFT of classical distributions.

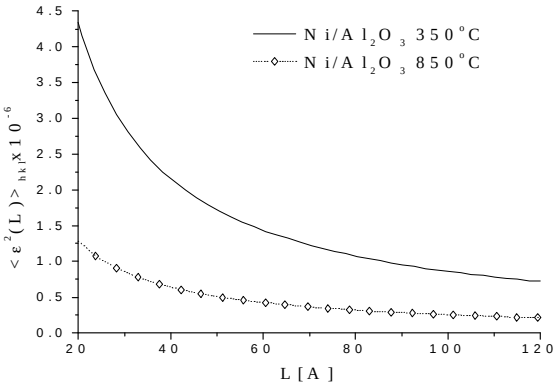

Fig. 7. The microstrain distribution functions.

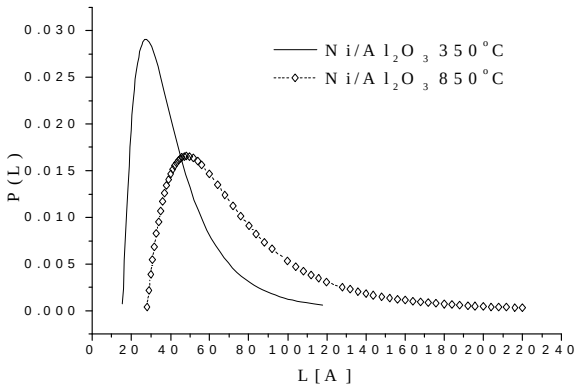

Fig. 8. The particles size distribution functions.

The main results regarding the investigated supported metal catalysts microstructures, are summarized in Table 3.

Table 3. Structural parameters of metal supported catalysts investigated.

Samples	Ni_{350^oC}				Ni_{350^oC}			
	GFF	V	pV	P7	GFF	V	pV	P7
D_{eff} [Å]	70	75	68	72	132	138	127	139
$\left\langle \varepsilon_{hkl}^2 \right\rangle \times 10^{-5}$	0.23548	0.22832	0.24259	0.21871	0.02549	0.02311	0.02733	0.02139
D_{arith} [Å]	42	45	41	43	75	77	76	80
D_{harm} [Å]	35	33	31	32	62	64	62	65
SFP %	3.87	3.52	3.97	3.61	2.34	2.28	2.51	1.97

D*eff* - effective particle size eq.(22)

$\left\langle \varepsilon_{hkl}^2 \right\rangle$ - mean square of the microstrain for $L = \frac{D_{eff}}{2}$,eq.(21)

D*arith* - arithmetic average particle size eq.(26)
Dharm - harmonic average particle size eq.(27)
SFP - stacking fault probability (1.5α + β) eq.(28)

The microstrain and particle size distribution functions were calculated using equations (21) and (24) and they are plotted in Figs. 7 and 8.

6. Conclusions

The GFF as a new approximation offers several advantages with respect to the traditional method of Fourier analysis. The conclusions that can be drawn from the study are as follows:

(i) The propagated errors occurring in classical sampling analysis (such as: background corrections, angular range of observation and the number of equally spaced points at which the diffraction line intensity is measured) are eliminated;

(ii) Our numerical results show that GFF can successfully treat asymmetric shapes of the XRLP and from mathematical point of view is simpler than Voigt, pseudo-Voigt or Pearson VII approaches.

(iii) Analytical formula of the integral width for true sample can successfully be used in Scherrer method for crystallite size evaluation.
(iv) Analytical formula of Fourier transform of true sample can be used in Warren-Averbach or Charlson methods.

Acknowledgements

The authors gratefully acknowledge our colleague Dr. P. Marginean for preparing the samples.

References

[1] B. E. Warren, X-Ray Diffraction, (Reading MA Addison-Wesley, 1969).
[2] E. J. Charlson, Ding-Hua Hu, M. R. Farukhi, Adv. X-ray Anal. **14**, 441 (1971).
[3] N. Aldea, E. Indrea, Comput. Phys. Commun. **60**, 155 (1990).
[4] N. Aldea, R. Zapotinschi, Progress in Catalysis **4**, 61 (1995).
[5] N. C. Popa, D. Balzar, J. Appl. Cryst. **35**, 338 (2002).
[6] R. A. Young, R. J. Gerdes, A. J. C. Wilson, Acta Cryst. **22**, 155 (1967).
[7] N. Aldea, Proceedings of the National Conference on Catalysis, Section C, p.76. Ploiesti, Romania 1995.
[8] D. Balzar, H. J. Ledbetter, Appl. Cryst. **26**, 97 (1993).
[9] R. W. Cheary, A. Coelho, J. Appl. Cryst. **25**, 109 (1992).
[10] H. Toraya, Powder Diffraction **4**(3), 130 (1989).
[11] R. A. Young, The Rietveld Method, (IUCr/Oxford Univ. Press., 1993).
[12] A. Losev, Preliminary Proceedings, Ninth Summer School on Computing Techniques in Physics, Skalsky Dvur, 1991.
[13] N. Aldea, C. V. Tiusan, R. Zapotinschi, Proceedings of the 8th joint EPS-APS International Conference on Physics Computing, 1996.
[14] N. Aldea, Andreea Gluhoi, P. Marginean, C. Cosma, Xie Yaning, Spectrochim Acta Part B **55**, 997 (2000).
[15] N. Aldea, Andreea Gluhoi, P. Marginean, C. Cosma, Xie Yaning, Hu Tiandou, Whongua Wu, Baozhong Dong, Spectrochim. Acta Part B **57**, 1453 (2002).
[16] B. E. Warren, B. L. Averbach, J. Appl. Phys. **21**, 595 (1950).
[17] R. L. Rothman, J. B. Cohen, Adv. X-ray Anal. **12**, 208 (1969).
[18] C. N. J. Wagner, E. N. Aqua, Adv. X-ray Anal. **7**, 46 (1964).
[19] N. Aldea, R. Zapotinschi, C. Cosma, Fresenius J. Anal. Chem. **355**, 367 (1995).
[20] J. P. Estrera, W. M. Duncan, S. R. Slughter, Computers in Physics **6**, 360 (1992).